ISSN 2321-807X
Volume 12 Number5
Journal of Advances in Chemistry

Synthesis and characterization of some new ruthenium (II) complexes as photosensitizers in dye-sensitized solar cells.

Ahmed H. Osman, Waleed A. El-Said and M. Abd El-Shakour

Department of Chemistry, Faculty of Science, Assiut University, Assiut, 71516, Egypt

Email: ahosman@aun.edu.eg

ABSTRACT

New ruthenium (II) complexes, $[Ru(DHZ)_2(bpy)]$, $[Ru(SCN)_2(bpy)(DMSO)_2]$, $[Ru(SCN)_2(dmbpy)(DMSO)_2]$ and $[RuCl_2(salen)]^{-2}$, where bpy = 2,2'- bipyridine, DHZ = 1,5-diphenylthiocarbazone, dmbpy = 4,4'-dimethyl-2,2' bipyridine and salen = 2,2'-ethylenebis(nitrilomethylidene)diphenol were synthesized and characterized by elemental analysis, FTIR, UV-Vis spectroscopy and thermal analysis. From data of these investigations the structural formula and the mode of bonding were obtained. These complexes were successfully applied to sensitization of nano-crystalline TiO_2 based solar cells (DSSCs). The photovoltaic efficiencies of the studied DSSCs increase in the following order $[Ru(DHZ)_2(bpy)]$< $[Ru(SCN)_2(bpy)(DMSO)_2]$< $[Ru(SCN)_2(dmbpy)(DMSO)_2]$< $[RuCl_2(salen)]^{-2}$. This increase is in agreement with the light harvesting of these complexes as indicated from their absorption spectra. Ferrioxalate complex enhanced the performance of some investigated cells. Therefore, a mechanism of this improvement has been postulated. Polyaniline as well as iodine doped polyaniline modified FTO electrode has been tested as promising counter electrodes. The efficiencies of the cells using iodine doped polyaniline is higher than that of polyaniline, which is assignable to the high conductivity of iodine.

Keywords

Dye-sensitized solar cells, Ruthenium complexes, PANI, $K_3[Fe(C_2O_4)_3]$.

Academic Discipline And Sub-Disciplines

Chemistry

SUBJECT CLASSIFICATION

Inorganic chemistry

TYPE (METHOD/APPROACH)

Ruthenium complexes-Dye sensitized solar cells

1. INTRODUCTION

Dye-sensitized solar cells (DSSCs) have attracted considerable attention in recent years due to the possibility of low-cost conversion of photovoltaic energy[1,2]. DSSCs possess four components: (i) dye sensitizer to harvest solar energy and generate excitons, (ii) nanostructure metal oxide material to transport electrons efficiently, (iii) redox couple, usually comprised of iodide/ triiodide (I^-/I^-_3) to reduce the oxidized dye back to its neutral state and (iv) counter electrode to accept the positive charge from the redox electrolyte. The following reactions summarize the working principles of the cell in a lucid manner, where S refers to the sensitizer [3-5]:

ISSN 2321-807X
Volume 12 Number5
Journal of Advances in Chemistry

$$S + h\nu \xrightarrow{\text{Light absorption}} S^* \quad (1)$$

$$S^* \xrightarrow{\text{Electron injection}} S^+ + e^- \quad (2)$$

$$I^-_3 + 2\,e^- \longrightarrow 3I^- \quad (3)$$

$$S^+ + 3/2\,I^- \longrightarrow S + 1/2\,I^-_3 \quad (4)$$

Due to the non-toxicity, availability and low-cost characteristics, TiO_2 has been the mostly preferred as the semiconductor for the photoelectrode. Although a lot of dyes have been tested and investigated, ruthenium complexes have proved to be the most effective consistently [6]. Therefore, we reported herein, the synthesis and characterization of some new ruthenium (II) complexes and study of their photovoltaic properties in DSSCs. Recently, nanostructured conducting polymers have been utilized as a potential catalyst for counter electrodes in DSSCs [7,8]. Among conductive polymers, polyaniline (PANI) is especially promising because its extremely low cost, good conductivity and good electro-catalytic activity [9-12]. Therefore, polyaniline prepared electrochemically (EC-PANI), polyaniline prepared chemically (C-PANI), iodine-doped polyaniline (I_2-PANI) as well as graphite have been tested in our DSSCs. Independently, ferrioxalate complex has been used in order to improve the performance of the cells.

2. EXPERIMENTAL

2.1 Materials and methods

All chemicals and solvents used were of analytical grade and used without any purifications. Fluorine-doped tin oxide substrate(FTO) (50mm x 50mm x 3 mm and with surface resistivity ~8Ω/sq was obtained from Sigma Aldrich.$[RuCl_2(DMSO)_4]$[13] , $[RuCl_2(bpy)(DMSO)_2]$ and $[RuCl_2(dmbpy)(DMSO)_2]$ complexes [14,15] were prepared according to the previously published work.

2.2 Synthesis of complexes

$[Ru(DHZ)_2(bpy)]$ was synthesized by adding an ethanolic solution of dithizone (0.106gm,0.413mmol) to an ethanolic solution of $[RuCl_2(bpy)(DMSO)_2]$ (0.1gm,0.207mmol). The reaction mixture was stirred at reflux for 8h under nitrogen and reduced light. During the reflux, the color of the solution turned to dark violet. After cooling to room temperature, the mixture was filtered and the filtrate was concentrated under vacuum to ~5 ml. A dark violet precipitate is formed by adding diethyl ether. The precipitate was filtered off, washed several times with diethyl ether and dried at 60^0C. (Calculated for $RuC_{36}N_{10}S_2O_{1.5}H_{33}$,FW = 794.929: C = 54.39,N = 17.62,S = 8.07,H = 4.19 %. Found: C = 50.88, N = 16.12, S = 6.30, H = 6.40 %).

$[Ru(SCN)_2(bpy)(DMSO)_2]$ was synthesized by adding an ethanolic solution of NH_4SCN (0.017gm, 0.22mmol) to well stirred solution of $[Ru(bpy)Cl_2(DMSO)_2]$ (0.0534gm, 0.11mmol) in ethanol. The reaction mixture was refluxed under nitrogen and reduced light for 8h. During the reaction, the color of the mixture turned from orange to brown. After cooling to the room temperature, a brown

precipitate was formed, filtered off, washed several times with ethanol and finally dried at 60 °C. (Calculated for $RuC_{16}N_4S_4O_2H_{20}$, FW = 529.692 : C = 36.28, N =10.58, S = 24.196, H = 3.8%. Found: C = 35, N =12.16, S = 21.3, H = 3.50%.

$[Ru(SCN)_2(dmbpy)(DMSO)_2]$ was synthesized by adding an ethanolic solution of NH_4SCN(0.07gm, 0.91mmol) to a well stirred solution of $[RuCl_2(dmbpy)(DMSO)_2]$ (0.2138gm, 0.453mmol) in ethanol. The reaction mixture was refluxed under nitrogen and reduced light for 8h. During the reflux, the color turned from orange to brown. After the completion of the reaction, the solution is cooled to room temperature, the formed precipitate is filtered off, washed with ethanol several times and dried at 60^0C. (Calculated for $RuC_{18}N_4O_2S_4H_{24}$, FW = 557.746 : C = 38.76, N = 10.05,S = 22.99, H= 4.34%. Found: C= 37.338, N = 11.6, S = 21.063, H = 3.83%).

$[RuCl_2(salen)]^{-2}$ was synthesized by adding a methanolic solution of salen (0.166gm, 0.62mmol) to $[RuCl_2(DMSO)_4]$ (0.3gm, 0.62 mmol) dissolved in CH_2Cl_2**.** The reaction mixture was stirred for 30 minutes at room temperature to get a clear solution. The mixture is refluxed for 10h under nitrogen atmosphere and reduced light. The reaction mixture is cooled to room temperature, filtered and the filtrate was evaporated to dryness, the residual solid was dissolved in CH_2Cl_2. A green precipitate formed by the addition of hexane was filtered off, washed with hexane several times and finally dried at room temperature.

Calculated for $RuC_{16}N_2O_7Cl_2H_{26}$, FW = 530.09 : C = 36.25, N = 5.28, H= 4.94 %. Found: C= 37.17, N = 5.54, H = 5.35 %).

2.3 Preparation of polyaniline modified FTO electrode

C-PANI was prepared according to previously published work[16-20]. Accurately, 0.5gm of aniline-HCl was dissolved in 15ml of distilled water(solution A) and 1.5gm of ammonium persulphate was dissolved in 15ml of distil-water (solution B), the two solutions A and B were stirred for 1h and then solution B was added to solution A drop wise and stirred for 1h, then the solution is kept to complete polymerization. FTO electrode was immersed in the polymer solution for one day. The polymer attached to the nonconductive side of FTO was removed. Finally, the electrode was dried at 60ºC. The prepared polymer was characterized by X-ray diffraction (XRD) and Fourier transient infrared (FT-IR).

The electrodeposited polyaniline (EC-PANI) was prepared according to previously published papers [7,17] with slight modification. FTO acted as a working electrode in three electrode system (a platinum as a counter electrode and Ag/AgCl as a reference electrode) on an electrochemical station (Autolab PGSTAT302F, Metrohm UK, and Ireland). The anodic deposition was controlled in a solution containing 0.3ml of aniline and 0.5ml of HCl (37%). The EC-PANI was prepared by controlling the number of cycles (72) with a potential range from 1 V to -0.3 V and a scan rate of 0.05 V/S, the resulting electrode was washed with distilled water and dried at 60 °C.

2.4 Preparation of iodine doped polyaniline (I_2-PANI)

Iodine doped PANI (I_2-PANI) counter electrode was prepared by immersing the PANI prepared chemically electrode in a solution of iodine in acetonitrile (10^{-3}M) for 6 h according to previously reported work [21-23].

2.5 Fabrication of DSSCs

Fluorine doped tine oxide glass (FTO) was cut into pieces of 2.5 cm x 2.5 cm size and cleaned [32].The photoanode was prepared by taking 200µLof TiO_2 paste and spin coated with speed 1500rpm for 50 seconds, then the substrate was heated at 80ºC and calcined for 60 min at 500°C. The photoanode is then immersed in a solution of $1x10^{-4}$ M sensitizers for 24h. For studying the effect of the addition of $K_3[Fe(C_2O_4)_3]$, the photoanode is immersed in a solution of $1x10^{-4}$M of both Ru complexes and iron complex. The DSSC was assembled by sandwiching the electrolyte (0.5M of KI and 0.05M of I_2 in ethylene glycol) between photoanode and counter electrode. The current-voltage characteristics of the DSSCs were measured using solar simulator with an AM1.5 spectral filter, and the intensity was adjusted to 1 sun(100 mW/cm^2)using calibrated cell. The output current and voltage were measured using a multimeter in the presence of variable resistance. The active surface area of the developed cell was $2.56cm^2$.

2.6 Instruments and measurements

The elemental analysis of the sensitizers was obtained using Elementar Vario EL C.H.N.S analysis system Gmblt Donaustr-7-D-63452 Hanau. The Fourier transient infrared(FT-IR) of prepared complexes was monitored using Nicolet 6700 FT-IR. . The corresponding spectra of the sensitizers were obtained using UV-visible spectrophotometer (Perkin Elmer instrument(Lambada 35 UV/Vis spectrometer)). The thermal analysis was obtained using DTG-60H, simultaneous DTA-TG apparatus, Shimadzu DSSCs cells were irritated by the solar simulator(ARC lamp power supply model 69920) with incident light intensity $100mW/cm^2$, which was calibrated with Si cell(Oriel instruments, Stratford, CT.U.S.A, model 91150V). The output current and voltage from the cell were measured using a digital multimeter.

3. RESULTS AND DISCUSSIONS

The synthesis of the precursor complex $[RuCl_2(DMSO)_2]$ was achieved as a yellow precipitate by the action of microwave on a solution of $RuCl_3$ in DMSO at 135 °C as previously reported [13]. The reactions of this yellow complex with the corresponding ligand yield the studied complexes through the substitution of DMSO or Cl^- as illustrated in scheme 1.

3.1 FTIR and electronic spectra

The FTIR spectroscopy has been shown to be a powerful tool to give structural information about the complexes. Figure 1 shows the typical I.R spectra of the studied complexes in range 4000-500 cm^{-1}. The characteristic vibrational frequencies of $[Ru(DHZ)_2(bpy)]$ have been identified by comparing the peaks of the complex with that of the free ligands (Fig. 1a). The strong band at 1438 cm^{-1} assigned to ν-(N=N) in the free dithizone is shifted to 1444 cm^{-1} in the complex; also, the two bands assigned to ν-(C=S) and ν-(C=N) were shifted from 891 cm^{-1} and 1589 cm^{-1} to 763 cm^{-1} and 1596 cm^{-1}, respectively indicating the coordination of dithizone with ruthenium[24]. The coordination of ruthenium with 2,2'-bipyridine is indicated by the shift of the two characteristic bands of free 2,2'-bipyridine from 1578 cm^{-1} and 1557 cm^{-1} to 1520 cm^{-1} and 1500 cm^{-1}, respectively in the complex[25,24]. Finally, the disappearance of the two characteristic bands of ν-SO at 1091cm^{-1} and 1013 cm^{-1} for DMSO indicate the complete substitution of DMSO[26].

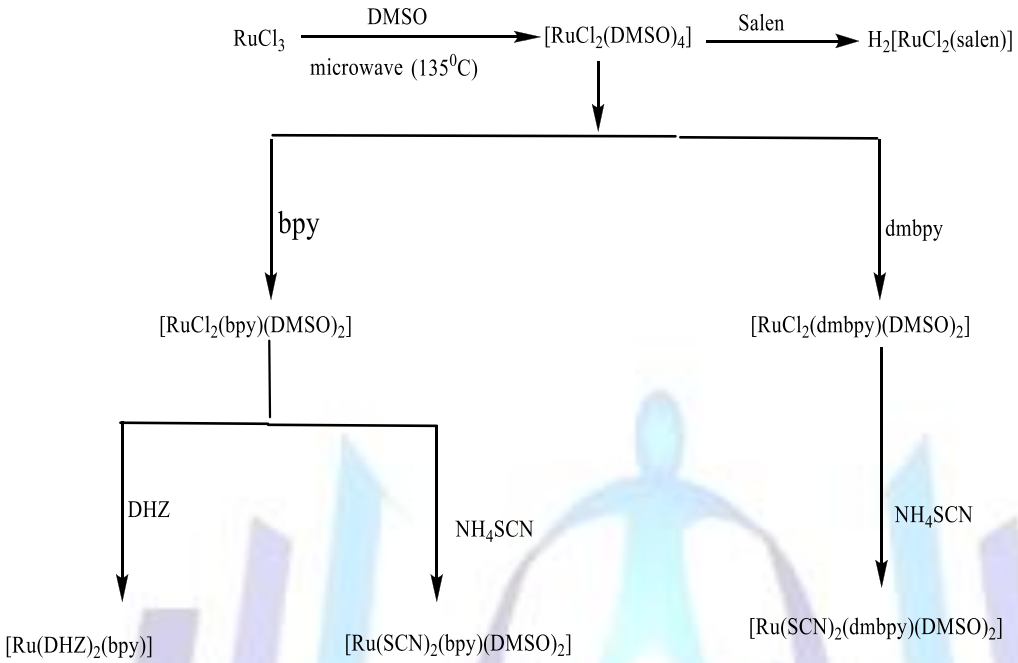

Scheme 1

The FTIR of the complexes $[Ru(SCN)_2(bpy)(DMSO)_2]$ and $[Ru(SCN)_2(dmbpy)(DMSO)_2]$ are shown in Fig. 1 (b,c), which show nearly the same peaks for the two complexes due to the similarity in their structures. The spectrum shows an intense and sharp peak at 2107 cm^{-1}, which is assignable for coordinated SCN in the complex [27,24,28]. The coordination of ruthenium with 2,2'-bipyridine is clarified by the shift of characteristic peaks for the free 2,2'-bipyridine from 1578cm^{-1}, 1557cm^{-1} to 1464cm^{-1}, and 1445cm^{-1} in $[Ru(SCN)_2(bpy)(DMSO)_2]$ and to 1558 cm^{-1},1540 cm^{-1} in $[Ru(SCN)_2(dmbpy)(DMSO)_2]$, which indicate the coordination of 2,2'-bipyridine[25,24]. Finally, the presence of coordinated DMSO in the complex is indicated by the presence of two characteristic peaks for ν–SO at 1088cm^{-1} and 1013cm^{-1} of DMSO[26].

Fig. 1 (d) demonstrated the I.R of $[RuCl_2(salen)]^{-2}$. The complexation of salen ligand with ruthenium is proved by the shift in ν-C=N peak from 1636 cm^{-1} for the free salen to 1597 cm^{-1}. The two peaks at 681 cm^{-1} and 425 cm^{-1} are attributable to the binding of ruthenium with N and O, respectively[29,28].

The UV-Vis absorbance spectra of the studied complexes were recorded at room temperature using ethanol or DMF as a solvent and are shown in Fig. 2 and the assignments of the bands are reported in table 1[29-33].

ISSN 2321-807X
Volume 12 Number5
Journal of Advances in Chemistry

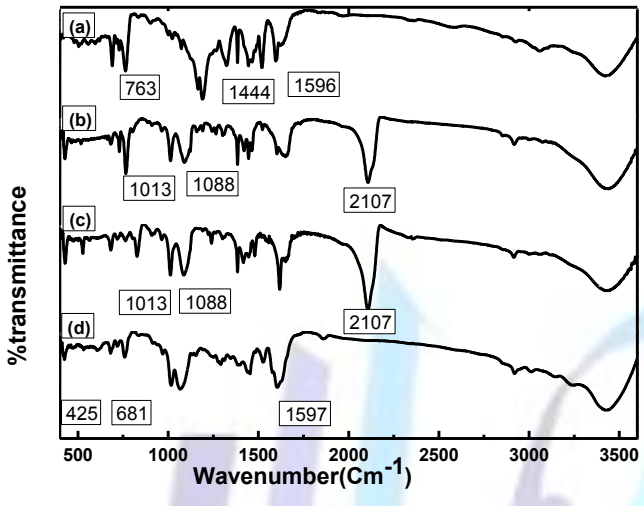

Fig. 1 FTIR of (a) [Ru(DHZ)$_2$(bpy)], (b)[Ru(SCN)$_2$(bpy)(DMSO)$_2$], (c)[Ru(SCN)$_2$(dmbpy)(DMSO)$_2$] and (d) [RuCl$_2$(salen)]$^{-2}$.

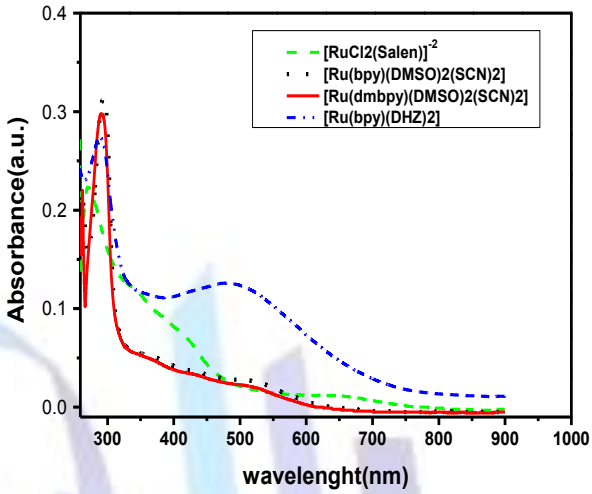

Fig. 2 UV-Vis spectroscopy of the studied complexes.

Table 1 UV-Vis spectroscopic data of complexes.

Complex	ν_{max}(cm^{-1})	ε*(10^3) (L cm^{-1} mol^{-1})	Assignment
[Ru(DHZ)$_2$(bpy)]	20283	12.6	π,π* (dithizone)
	34482	27.6	Intra-ligand
[Ru(SCN)$_2$(bpy)(DMSO)$_2$]	19801	2.7	MLCT
	34246	31.3	Intra-ligand
[Ru(SCN)$_2$(dmbpy)(DMSO)$_2$]	19880	2.4	MLCT
	34129	29.5	Intra-ligand
[RuCl$_2$(salen)]$^{-2}$	15384	1.1	MLCT
	37037	22.1	Intra-ligand

ISSN 2321-807X
Volume 12 Number5
Journal of Advances in Chemistry

3.2 Thermal behavior

The thermal behavior of the studied complexes was carried out within the temperature range from room temperature up to 1000 °C on a dynamic air atmosphere using thermogravimetric analysis (TGA) and differential thermal analysis (DTA). The observed mass losses are based on the TG results, and the calculated mass losses are based on the molecular weight of the proposed formula. The TG curve of $[Ru(DHZ)_2(bpy)].1.5\ H_2O$ (Fig. 3 a) shows three steps of decomposition. The first step at 38-216 °C corresponds to the loss of 1.5 water molecules of hydration (calc. 3.4 %, found 3.31 %). The anhydrous complex decomposes in a major stage consisting of three steps corresponds to the stepwise decomposition of the complex ended with oxide formation. The percentage weight of the residue agrees well with the RuO_2 formation (calc. 16.75 %, found 17.12 %). The $[Ru(SCN)_2(bpy)(DMSO)_2]$ complex was found to decompose in three steps (Fig. 3 b), associated with the stepwise decomposition of the complex. The residue may belong mostly to RuS_2 (calc. 31.19 %, found 30.81 %). This result in agreement with the decomposition of some ruthenium complexes [34,35]. The formation of sulfide residue rather than oxide could be attributed to the high sulfur content of the complex under investigation. The $[Ru(SCN)_2(dmbpy)(DMSO)_2]$ complex was found to decompose in three steps with the temperature range 20-400 °C. The residue percentage corresponding to RuS_2 formation (calc. 29.62 %, found 29.73 %) as the above-mentioned complex. The TG curve of $[RuCl_2(salen)]^{-2}.5H_2O$ exhibits three steps. The first step in the temperature range 29-216 °C, corresponding to the evolution of five water molecules (calc. 17.05 %, found 16.46 %). The major step (58.75 %) occurs within the temperature range 220-400 °C corresponding to un-assignment ligand decomposition. The weight loss percentage of the residue could be assigned to a mixture of the ruthenium oxide and metallic ruthenium.

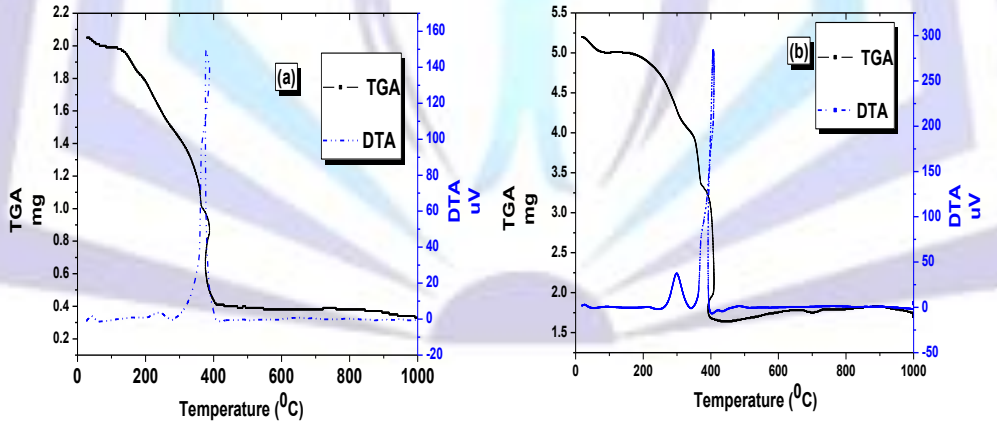

Fig. 3 TGA and DTA curves of (a)$[Ru(DHZ)_2(bpy)]$ and (b) $[Ru(SCN)_2(bpy)(DMSO)_2]$ complexes.

Based on the above arguments the chemical structures as shown in Fig. 4 are suggested for the prepared complexes.

3.3 Photovoltaic performance of the studied DSSCs

The performance of a solar cell is defined by several parameters: open-circuit voltage (Voc), short-circuit current density (Jsc) and fill factor (FF). The output efficiency (%ɳ) calculated using the following equations:

$$\eta(\%) = \frac{Jsc.Voc.FF.100}{Pin} \qquad FF = \frac{Pmax}{Jsc.Voc}$$

where Voc, is the maximum voltage obtained at zero current; Jsc is the short-circuit current which is the maximum current obtained under less resistance (short-circuit) conditions, Pin is the solar incident power= (100mW/cm^2) (one sun = 1.5 A.M) and P_{max} is the maximum power generated from the cell ($P_{max} = I_{max} \times V_{max}$).

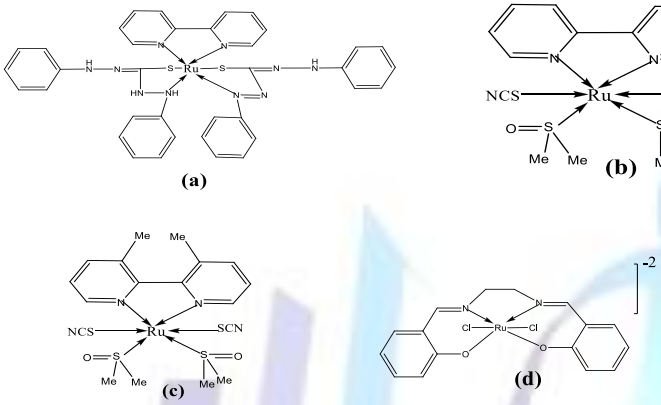

Fig. 4 Proposed structures of the studied complexes; (a) [Ru(DHZ)$_2$(bpy)], (b) [Ru(SCN)$_2$(bpy)(DMSO)$_2$], (c) [Ru(SCN)$_2$(dmbpy)(DMSO)$_2$] and (d) [RuCl$_2$(salen)]$^{-2}$.

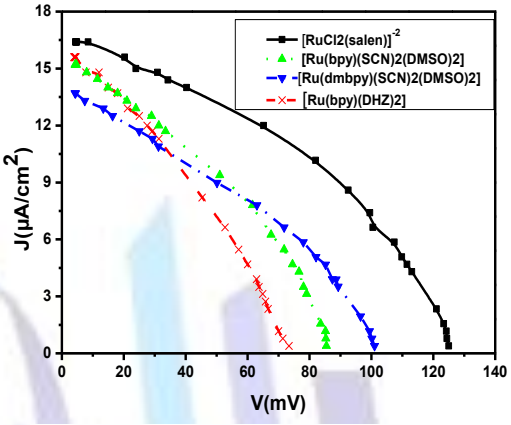

Fig. 5 J-V curves of DSSCs of the studied complexes using I$_2$-PANI as a counter electrode.

The photocurrent density –voltage curves of the DSSCs using ruthenium complexes under investigation are given in Fig. 5 (using I$_2$-PANI) as a counter electrode. The results are recorded under A.M 1.5G simulated sun light at a light intensity 100mW/cm^2. The data are given in details in table 2 The photovoltaic efficiencies of used sensitizers increase in the following order [Ru(DHZ)$_2$(bpy)]<[Ru(SCN)$_2$(bpy)(DMSO)$_2$]<[Ru(SCN)$_2$(dmbpy)(DMSO)$_2$]< [RuCl$_2$(salen)]$^{-2}$.

Table 2 Photovoltaic parameters of the studied DSSCs of the complexes using I$_2$-PANI as a counter electrode.

Complex	Jsc(μA/cm^2)	Voc(mV)	%η(10^{-4})	FF
[RuCl$_2$(Salen)]$^{-2}$	16.4	125	8.3	0.405
[Ru(SCN)$_2$(dmbpy)(DMSO)$_2$]	13.7	101	4.84	0.35
[Ru(SCN)$_2$(bpy)(DMSO)$_2$]	15.2	85.5	4.79	0.369
[Ru(DHZ)$_2$(bpy)]	15.6	73.4	3.7	0.325

ISSN 2321-807X
Volume 12 Number5
Journal of Advances in Chemistry

These results are in agreement with the light harvesting of the complexes as shown in their absorption spectra (Fig. 2); except in the case of [Ru(DHZ)$_2$(bpy)], which shows an intense visible absorption band at 290 nm and 493 nm (table 1). This absorption is associated with the delocalized electronic system of the dithizone ligand [36]. The presence of this delocalization may be responsible for the low efficiency exhibited by the dithizone complex, the presence of such low laying energy level may enhance the deactivation of the excited state formed upon light absorption and consequently competes with the electron injection to the conduction band of TiO_2 (reaction 2) as explained in Fig.6.

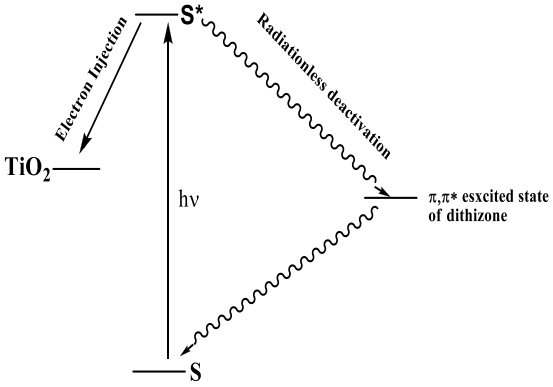

Fig. 6 Radiationless deactivation of the excited state in case of [Ru(DHZ)$_2$(bpy)].

The low cell performances obtained (table 2) may result from the relatively poor interconnection between the nanocrystalline TiO_2 (reaction 2) and sensitizers under investigation. This poor interconnection is associated with the absence of any anchoring group in the complex, like the carboxylic or phosphonic group, which is the most decisive factors in bringing the relative orientation of energy level of donor and acceptor during the attachment on the metal oxide, which leads to increase the electron injection efficiency. Sensitizers also show slower electron injection or self-quenching if they undergo aggregation, which can be encountered either before or during processing of dye adsorption onto metal oxide.

3.4 Effect of addition of $K_3[Fe(C_2O_4)_3]$

Additives play a central role in the enhancement of photoelectrochemical performance of DSSCs. Most additives are understood at the fairly phenomenological level, and their effects are often attributed to modification of redox couple potentials band shifts of the semiconducting electrode material, effect of surface blocking or surface dye organization [37].

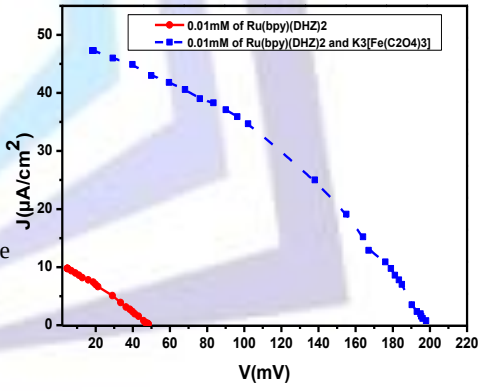

Fig. 7 J-V curve of DSSCs of [Ru(DHZ)$_2$(bpy)] in absence and in presence of $K_3[Fe(C_2O_4)_3]$ using C-PANI as a counter electrode.

Our investigations on the effect of the addition of $K_3[Fe(C_2O_4)_3]$ complex demonstrated an increase in cell performance in case of [Ru(DHZ)$_2$(bpy)] (Fig. 7 and table 3). This enhancement effect can be attributed to two roles: firstly, the addition of this ferrioxalate complex to the ruthenium complex leads to increase in the light absorption, assignable to the formation of charge transfer (CT) complex of ferrioxalate complex and ruthenium complex as indicated by the development of a new absorption of their mixture (Fig. 8).

The formation of such CT complex leads to increase the light –harvesting capability of the cell, giving rise to increasing the efficiency of the cell. Secondly, light excitation of $K_3[Fe(C_2O_4)_3]$ leads to a photolysis of this complex, as a result of ligand-metal charge transfer (LMCT) according to the following photoreactions:

$$[Fe^{III}(C_2O_4)_3]^{3-} \xrightarrow[LMCT]{h\nu} [(\dot{C}_2O_4)Fe^{II}(C_2O_4)_2]^{3-} \quad (5)$$

$$[(\dot{C}_2O_4)Fe^{II}(C_2O_4)_2]^{3-} \longrightarrow Fe^{II}(C_2O_4)_2^{2-} + C_2O_4^{-\bullet} \quad (6)$$

Table 3 Effect of addition of $[K_3[Fe(C_2O_4)_3]$ on the photovoltaic parametersof DSSCs of $[Ru(DHZ)_2(bpy)]$ using C-PANI as a counter electrode.

Complex	Jsc(μA/cm^2)	Voc(mV)	% η (10^{-4})	FF
$[Ru(DHZ)_2(bpy)]$	9.8	48.4	1.47	0.31
$[Ru(DHZ)_2(bpy)]$+ferrioxalate complex	47.3	198	35.5	0.38

The formed oxalate radical, which is confirmed by electron paramagnetic resonance [38] adds another route in the reduction of the oxidized sensitizer to its neutral state; this is of course, beside the role of I^-/I_3^-couple as shown in the scheme (2).

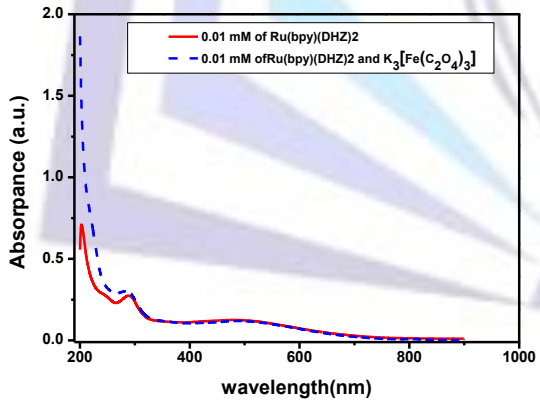

Fig. 8 UV-Vis spectroscopy of $[Ru(DHZ)_2(bpy)]$ in absence and in presence of $K_3[Fe(C_2O_4)_3]$.

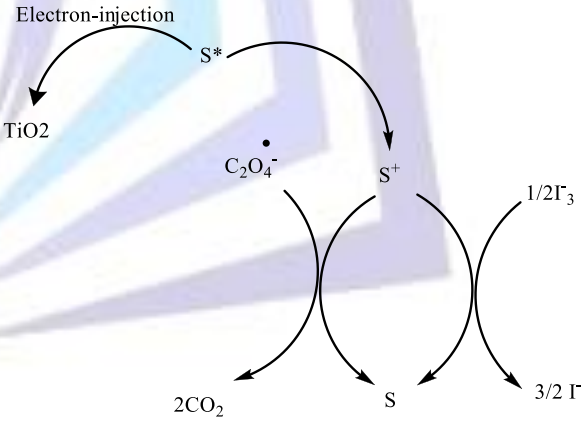

Scheme 2

It is well known that electron injection from the sensitizer into the TiO_2 typically happens in femtosecond to picosecond time scale whereas charge recombination in the microsecond to millisecond time scale [39]. The reduction of oxidized sensitizer molecules occurs in the ms or μs range, which in by several orders of magnitude slower than injection rate. Also, the transient state formed by

light absorption of $K_3[Fe(C_2O_4)_3]$ was found to reached its maximum intensity 2.6 ps after excitation then remains constant for at least 4ns [40]. Upon comparison of the times mentioned above, it is clear that the ferrioxalate complex will play an enhancement effect of the performance of the DSSCs if there is a good interaction between it and the sensitizer. Therefore, this point will be subject to further investigations in the future. Specially, we have recently proved an enhancement effect of this ferrioxalate complex on the photo colorization and photodegradation of an azo dye through UV/H_2O_2 advanced oxidation process [41].

In case of the complexes $[Ru(SCN)_2(bpy)(DMSO)_2]$, $[Ru(SCN)_2(dmbpy)(DMSO)_2]$, and $[RuCl_2(salen)]^{-2}$, the addition of ferrioxalate complex to their solutions lead to no improvement of their cell performances (as indicated by J-V curve (Fig. 9) and reported photovoltaic parameters (table 4) for $[RuCl_2(salen)]^{-2}$ as representative example). This results can be attributed to the poor electronic interaction between these complexes and the iron complex, as indicated by the absence of any new absorption of their mixture (Fig. 10), in contrast to the results of the above-mentioned examples

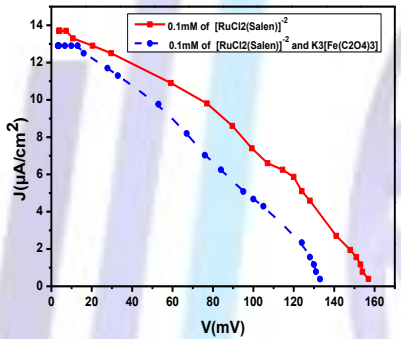

Fig. 9 J-V curve of DSSCs of $[RuCl_2(salen)]^{-2}$ in absence and in presence of $K_3[Fe(C_2O_4)_3]$ using C-PANI as a counter electrode.

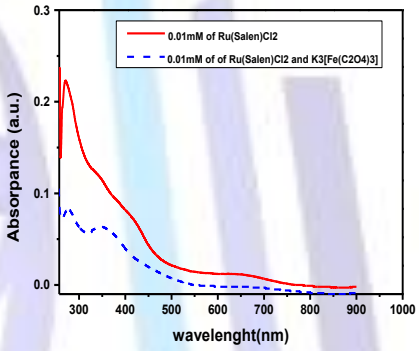

Fig. 10 U.V-Vis spectroscopy of $[RuCl_2(salen)]^{-2}$ in absence and in presence of $K_3[Fe(C_2O_4)_3]$.

Table 4 Effect of addition of $[K_3[Fe(C_2O_4)_3]$ on the photovoltaic parameters of DSSCs of $[RuCl_2(salen)]^{-2}$ using C-PANI as a counter electrode.

Complex	Jsc(μA/cm^2)	Voc(mV)	% η (10^{-4})	FF
$[RuCl_2(salen)]^{-2}$	13.7	157	7.74	0.36
$[RuCl_2(salen)]^{-2}$ + ferrioxalate complex	12.9	133	5.5	0.32

ISSN 2321-807X
Volume 12 Number5
Journal of Advances in Chemistry

3.5 Effect of kinds of counter electrode

In order to throw some light on the effect of kinds of counter electrodes, graphite, (EC-PANI), (C-PANI) and (I_2-PANI) have been examined. The results, as shown in fig.11 and reported in table 5, which demonstrated that the efficiency of the cell consist of $[RuCl_2(salen)]^{-2}$ as sensitizer increase in the following order: EC-PANI< graphite< C-PANI< I_2-PANI. Upon comparison of (EC-PANI), (C-PANI), the nanofiber shape and porous structure for (EC-PANI) is believed to a better electrocatalytic performance to I^-/I_3^-electrolyte. However, the separation of polymer from FTO substrates offers a high interfacial resistance is an unfavorable factor for charge transportation.

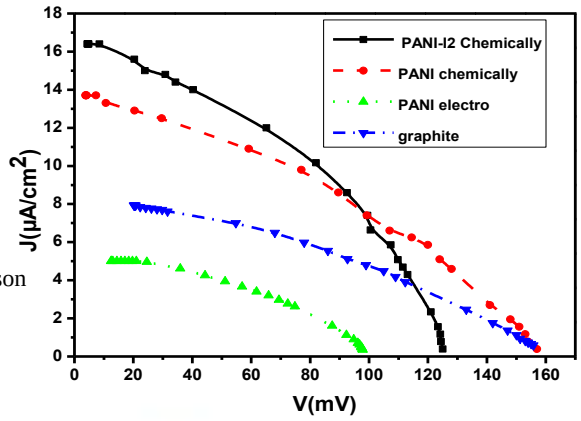

Fig. 11 J-V curves of DSSCs of $[RuCl_2(salen)]^{-2}$ using different counter electrodes.

Independently, cathodic reduction peak for (C-PANI) is higher than (EC-PANI), which means that electrocatalytic activity of (C-PANI) is better than (EC-PANI)[17]. I_2-PANI occupies the top position in the above series, which can be associated to the high conductivity of iodine doped in this polymer.

Table 5 The effect of kind of counter electrodes on the cell performance using [Ru Cl_2(salen)]$^{-2}$ a photosensitizer.

Counter electrode	Jsc(μA/cm^2)	Voc(mV)	%η(10^{-4})	FF
I_2-PANI	16.4	125	8.3	0.405
C-PANI	13.7	157	7.7	0.36
EC-PANI	5	97.9	2.1	0.43
Graphite	7.93	155.8	4.82	0.39

4. Conclusion

It is clear that the $[RuCl_2(salen)]^{-2}$ complex showed the highest efficiency compared to other complexes, which is due to the good light harvesting ability of this complex as indicated from UV-Vis absorption spectra of complexes. By adding $K_3[Fe(C_2O_4)_3]$ complex to the used complexes to improve their photovoltaic response, the efficiency of $[Ru(DHZ)_2(bpy)]$+ K3[Fe(C2O4)3] system only increased by 24 times compared to $[Ru(DHZ)_2(bpy)]$ system, while the other complexes efficiency decreased. This decrease in $[Ru(SCN)_2(bpy)(DMSO)_2]$, $[Ru(SCN)_2(dmbpy)(DMSO)_2]$, and $[RuCl_2(salen)]^{-2}$ efficiency is related to the poor electronic interaction

of these complexes and absence of any new absorption of their mixture. Finally, the I_2-PANI counter electrode shows the highest efficiency compared to C-PANI, EC-PANI and graphite. This is due to the presence of doped iodine, which raises the conductivity of the PANI.

ACKNOWLEDGMENTS

The authors gratefully acknowledge the financial support of this work by Assiut university.

Refernces:

1. Ye M, Wen X, Wang M, Iocozzia J, Zhang N, Lin C, Lin Z (2015) Recent advances in dye-sensitized solar cells: from photoanodes, sensitizers and electrolytes to counter electrodes. Materials Today 18 (3):155-162

2. Gonçalves LM, de Zea Bermudez V, Ribeiro HA, Mendes AM (2008) Dye-sensitized solar cells: A safe bet for the future. Energy & Environmental Science 1 (6):655-667
3. Karmakar AS, Ruparelia JP A Critical Review on Dye Sensitized Solar Cells.
4. Grätzel M (2003) Dye-sensitized solar cells. Journal of Photochemistry and Photobiology C: Photochemistry Reviews 4 (2):145-153
5. Nazeeruddin MK, Baranoff E, Grätzel M (2011) Dye-sensitized solar cells: a brief overview. Solar Energy 85 (6):1172-1178
6. Chandrasekharam M, Rajkumar G, Rao CS, Suresh T, Reddy MA, Reddy PY, Soujanya Y, Takeru B, Jun-Ho Y, Nazeeruddin MK (2011) Polypyridyl Ru (II)-sensitizers with extended π-system enhances the performance of dye sensitized solar cells. Synthetic Metals 161 (11):1098-1104 %@ 0379-6779
7. Zhang J, Hreid T, Li X, Guo W, Wang L, Shi X, Su H, Yuan Z (2010) Nanostructured polyaniline counter electrode for dye-sensitised solar cells: Fabrication and investigation of its electrochemical formation mechanism. Electrochimica Acta 55 (11):3664-3668
8. Tai Q, Chen B, Guo F, Xu S, Hu H, Sebo B, Zhao X-Z (2011) In situ prepared transparent polyaniline electrode and its application in bifacial dye-sensitized solar cells. Acs Nano 5 (5):3795-3799
9. Lee TH, Do K, Lee YW, Jeon SS, Kim C, Ko J, Im SS (2012) High-performance dye-sensitized solar cells based on PEDOT nanofibers as an efficient catalytic counter electrode. Journal of Materials Chemistry 22 (40):21624-21629
10. Jeon SS, Kim C, Ko J, Im SS (2011) Spherical polypyrrole nanoparticles as a highly efficient counter electrode for dye-sensitized solar cells. Journal of Materials Chemistry 21 (22):8146-8151
11. Trevisan R, Döbbelin M, Boix PP, Barea EM, Tena-Zaera R, Mora-Seró I, Bisquert J (2011) PEDOT nanotube arrays as high performing counter electrodes for dye sensitized solar cells. Study of the interactions among electrolytes and counter electrodes. Advanced Energy Materials 1 (5):781-784
12. Huang K-C, Hu C-W, Tseng C-Y, Liu C-Y, Yeh M-H, Wei H-Y, Wang C-C, Vittal R, Chu C-W, Ho K-C (2012) A counter electrode based on hollow spherical particles of polyaniline for a dye-sensitized solar cell. Journal of Materials Chemistry 22 (29):14727-14733
13. Harvey A, Draganjac M, Chui S, Snell R, Benjamin E (2009) Microwave Synthesis of cis-Dichlorotetrakis (dimethylsulfoxide) ruthenium (II). Journal of the Arkansas Academy of Science 63:185
14. Zakeeruddin SM, Nazeeruddin MK, Humphry-Baker R, Grätzel M, Shklover V (1998) Stepwise assembly of tris-heteroleptic polypyridyl complexes of ruthenium (II). Inorganic Chemistry 37 (20):5251-5259 %@ 0020-1669
15. Mulhern D (2003) Synthesis and characterisation of Ruthenium (II) tris (heteroleptic) complexes containing a triazole ligand. Dublin City University,
16. Stejskal J, Gilbert R (2002) Polyaniline. Preparation of a conducting polymer (IUPAC technical report). Pure and Applied Chemistry 74 (5):857-867
17. Wu J, Li Y, Tang Q, Yue G, Lin J, Huang M, Meng L (2014) Bifacial dye-sensitized solar cells: A strategy to enhance overall efficiency based on transparent polyaniline electrode. Scientific reports 4
18. Hobaica SC (2003) Stability of polyaniline in air and acidic water. Journal of Polymer Science Part B: Polymer Physics 41 (8):807-822
19. Atassi Y, Tally M, Ismail M (2008) Synthesis and characterization of chloride doped polyaniline by bulk oxidative chemical polymerization. Doping effect on electrical conductivity. arXiv preprint arXiv:08093552

20. El-Said WA, Yea C-H, Choi J-W, Kwon I-K (2009) Ultrathin polyaniline film coated on an indium–tin oxide cell-based chip for study of anticancer effect. Thin Solid Films 518 (2):661-667
21. Mathai CJ, Saravanan S, Anantharaman M, Venkitachalam S, Jayalekshmi S (2002) Effect of iodine doping on the bandgap of plasma polymerized aniline thin films. Journal of Physics D: Applied Physics 35 (17):2206
22. Padmanabhan P, Sreelatha K (2012) Iodine doped, semi-conducting nylon 6 polymers. Journal of Plastic Film and Sheeting:8756087912464036
23. Boddula R, Srinivasan P (2013) Use of iodine doped polyaniline salt in the stereoselective synthesis of 2-methyl-4-substituted-1, 2, 3, 4-tetrahydroquinoline derivatives. Catalysis Communications 30:56-60
24. Furniss BS (1989) Vogel's textbook of practical organic chemistry. Pearson Education India,
25. Razzak M, Karim MR, Hoq MR, Mirza AH (2015) New Schiff Bases from 6, 6'-Diformyl-2, 2'-Bipyridyl with Amines Containing O, S, N and F: Synthesis and Characterization. International Journal of Organic Chemistry 5 (04):264
26. Evans IP, Spencer A, Wilkinson G (1973) Dichlorotetrakis (dimethyl sulphoxide) ruthenium (II) and its use as a source material for some new ruthenium (II) complexes. J Chem Soc, Dalton Trans (2):204-209 %@ 1364-5447
27. Nazeeruddin MK, Zakeeruddin S, Humphry-Baker R, Jirousek M, Liska P, Vlachopoulos N, Shklover V, Fischer C-H, Grätzel M (1999) Acid-base equilibria of (2, 2'-bipyridyl-4, 4'-dicarboxylic acid) ruthenium (II) complexes and the effect of protonation on charge-transfer sensitization of nanocrystalline titania. Inorganic Chemistry 38 (26):6298-6305
28. Shaabani B, Darbari R (2013) Synthesis and characterization of salen and thiocyanate complexes with Co 2, Fe 3, Cu 2, and Mn 2 transition metal cations.
29. Bordini J, Hughes DL, Da Motta Neto JD, Jorge da Cunha C (2002) Nitric oxide photorelease from ruthenium salen complexes in aqueous and organic solutions. Inorganic chemistry 41 (21):5410-5416
30. Works CF, Ford PC (2000) Photoreactivity of the Ruthenium Nitrosyl Complex, Ru (salen)(Cl)(NO). Solvent Effects on the Back Reaction of NO with the Lewis Acid RuIII (salen)(Cl) 1. Journal of the American Chemical Society 122 (31):7592-7593
31. Campagna S, Puntoriero F, Nastasi F, Bergamini G, Balzani V (2007) Photochemistry and photophysics of coordination compounds: ruthenium. In: Photochemistry and Photophysics of Coordination Compounds I. Springer, pp 117-214
32. Rillema DP, Mack KB (1982) The low-lying excited state in ligand. pi.-donor complexes of ruthenium (II): mononuclear and binuclear species. Inorganic Chemistry 21 (10):3849-3854
33. Adeloye AO, Ajibade PA (2014) A high molar extinction coefficient Ru (II) complex functionalized with cis-Dithiocyanato-bis-(9-anthracenyl-10-(2-methyl-2-butenoic acid)-1, 10-phenanthroline): potential sensitizer for stable dye-sensitized solar cells. Journal of Spectroscopy 2014
34. Holló B, Krstić M, Sovilj SP, Pokol G, Szécsényi KM (2011) Thermal decomposition of new ruthenium (II) complexes containing N-alkylphenothiazines. Journal of thermal analysis and calorimetry 105 (1):27-32
35. Rocha FV, Barra CV, Franchi SJ, Netto AV, Mauro AE, Frem RC (2010) Study on the thermal behavior of the complexes of the type [PdX2 (tdmPz)](X= Cl−, Br−, I−, SCN−). Journal of thermal analysis and calorimetry 106 (2):385-389
36. Meriwether L, Breitner E, Sloan C (1965) The photochromism of metal dithizonates. Journal of the American Chemical Society 87 (20):4441-4448
37. Hagfeldt A, Boschloo G, Sun L, Kloo L, Pettersson H (2010) Dye-sensitized solar cells. Chemical reviews 110 (11):6595-6663
38. Ingram D, Hodgson W, Parker C, Rees W (1955) Detection of labile photochemical free radicals by paramagnetic resonance.
39. Sokolský M, Cirák J (2010) Dye-sensitized solar cells: materials and processes. Acta Electrotechnica et Informatica 10 (3):78-81
40. Chen J, Zhang H, Tomov IV, Wolfsberg M, Ding X, Rentzepis PM (2007) Transient structures and kinetics of the ferrioxalate redox reaction studied by time-resolved EXAFS, optical spectroscopy, and DFT. The Journal of Physical Chemistry A 111 (38):9326-9335

41. Ahmed Hassan Osman and Gamal Abdel-Wahab Ahmed(2015) Photochemical Oxidation of an Azo Dye in Aqueous Solutions by UV/H_2O_2 Process. Assiut university journal of chemistry (44):(99-105)